Soft Matter

PAPER

Cite this: DOI: 10.1039/c6sm00228e

Wrinkling of structured thin films *via* contrasted materials†

Dong Yan, Kai Zhang* and Gengkai Hu

Received 28th January 2016,
Accepted 13th March 2016

DOI: 10.1039/c6sm00228e

www.rsc.org/softmatter

Regular surface patterns induced by the wrinkling of thin films have received intense attention in both science and engineering. We investigate the wrinkling of structured thin films that consist of two types of materials arranged in periodic patterns. A mechanical model is proposed to understand the physics of the wrinkling, and a set of scaling laws for the wrinkle wavelength are obtained. Periodic wrinkles are generated in the local regions of structured films *via* in-plane contrasted elastic modulus between heterogeneous materials. The wrinkle morphology and location can be tailored by designing structured thin films in a controllable way. Our findings provide the basis for understanding the wrinkling of structured thin films and for the manufacture of regular surface patterns *via* wrinkling.

Introduction

Wrinkling induced by instability of thin films has received intense attention in recent years owing to its important applications in flexible electronics,[1,2] material science,[3–6] metrology,[7,8] biomedical engineering[9–13] and aerospace engineering.[14,15] There is also considerable interest in understanding the fundamental aspects of wrinkling,[16–24] including the wavelength and amplitude of wrinkles and the transition of wrinkle patterns. Most studies of the wrinkling only consider uniform films, no matter whether they are free-standing or bonded to a compliant substrate.[12,23–26] In fact, heterogeneous films widely exist in nature and engineering,[1–6,11–15,27–30] and the in-plane heterogeneous characteristics have an important role in determining the surface pattern of wrinkles on a film.[31–34] Recently, the wrinkling behaviors in patterned porous films and heterogeneous films have also been studied.[3–6,16–19] A simple method for studying the wrinkling of thin heterogeneous film is to stretch the film with clamped boundaries. It is reported that wrinkling of the film under stretching arises because the clamped stiff boundaries prevent the film from contracting laterally *via* the Poisson effect of the whole film.[12,23,25] However, boundaries of local regions of the film are also able to be constrained when the film is made up of different types of materials with contrasted in-plane elastic modulus. The physics of the wrinkling *via* the contrasted in-plane elastic modulus remains a challenge, and a method of generating controllable periodic patterns on the surfaces of thin heterogeneous films is also demanded. In this study, we investigate the wrinkling of heterogeneous films both experimentally and through numerical simulation and further reveal the underlying physics of wrinkling by developing a theoretical model, and by tailoring wrinkle morphology in a controllable way.

School of Aerospace Engineering, Beijing Institute of Technology, Beijing 100081, China. E-mail: zhangkai@bit.edu.cn

† Electronic supplementary information (ESI) available: The condition of inextensibility, numerical results for the wrinkling of structured films, the amplitude of wrinkles. See DOI: 10.1039/c6sm00228e

Experimental approach

In order to investigate the mechanism of wrinkling of a heterogeneous film, a structured film consisting of two different types of materials in a periodic arrangement is studied. As shown in Fig. 1a, a polyimide film is cut to a size of 180 × 60 × 0.025 mm (length × width × thickness). Rectangular elements with a length (L_e) of 20.0 mm and a width (W_e) of 10.0 mm are drawn on the film. By using a laser, holes with diameters of 0.15 mm, arranged in a regular hexagonal pattern with a porosity of 24.6%, are then punched on half of the rectangular elements in a checkerboard configuration. Thus, the microstructured element (R_1) can be considered as a composite material whose effective mechanical properties are different from those of the uniform

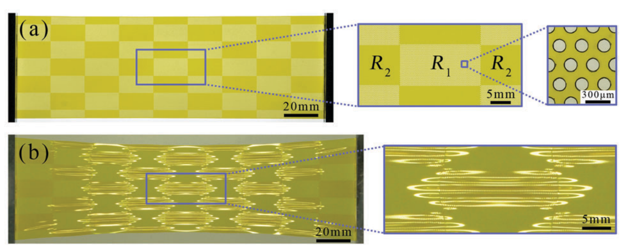

Fig. 1 (a) Structured thin film consisting of two different types of materials in a periodic arrangement. The structured film possesses a hierarchical structure, including a film structure, a periodic cell with four elements and a composite with periodic holes. (b) Wrinkle pattern of the structured film under stretching at 10% strain.

polyimide film. The structured film thus possesses a hierarchical structure, including a film structure, a periodic cell with four elements and a composite with periodic holes, as shown in Fig. 1a. The elastic modulus (E_2) of the uniform polyimide film is measured to be 2.88 ± 0.11 GPa by tensile testing, whereas the composite material with periodic holes has an effective elastic modulus (E_1) of 1.44 GPa, calculated by the finite element method (FEM). Poisson ratios (ν) for both materials are assumed to be 0.31 according to ref. 15. Then, the ends of the film are clamped with aluminum plates and stretched by the tensile machine (MTS, Eden Prairie, MN, USA) with a strain rate of 2% min^{-1}. Two lamps are placed in front of the film with an angle of about 45° or −45° to the normal of the film. A digital camera perpendicular to the film is used to capture the images of the film during stretching as shown in Fig. 1b.

Results and discussion

Qualitative observations

As shown in Fig. 1b, when the stretching strain (ε) is beyond a critical value, wrinkles with a wavelength (λ) are decorated in the regions of the composite material, whereas the central regions of the uniform material remain almost flat. Owing to the periodic configuration of the elements, wrinkles on the whole film exhibit checkerboard characteristics under the stretching. The wrinkles arch across the holes in the composite, and no local buckling occurs near the holes. The holes on the film are so small that the compressive stress induced by the holes cannot trigger the buckling of the local regions near the holes. When we change the length of the elements (L_e) or the ratio of elastic moduli of the two materials ($E_r = E_2/E_1$), a similar pattern of wrinkles is observed on the films, but the wavelength of the wrinkles in the elements is modified. For example, λ decreases from 3.43 mm to 2.85 mm with increasing E_r from 1.25 to 2.50 at 10% strain when L_e is fixed to 20.0 mm, as shown in Fig. 2a–d. As changing L_e from 12.5 mm to 30.0 mm with a fixed E_r of 1.50, λ increases from 2.74 mm to 3.78 mm at 10% strain (Fig. 2b, e and f). Wavelengths of different films during stretching are measured and plotted as shown in Fig. 2g. The wavelength is decreased as the stretching strain increases. The film with larger element length or smaller ratio of elastic moduli has a larger wavelength at the same strain level.

Wrinkling mechanism

When the uniform free-standing film is stretched, the film tends to contract laterally due to the Poisson effect of the whole film.[12,23,25] Preventing the contraction by stiff boundaries results in a field of compressive stress near the clamped ends and further triggers the wrinkling of the whole film. In comparison, the compressive stress in our structured film is mainly generated *via* in-plane contrasted elastic modulus between the elements, not the Poisson effect of the whole film. When a periodic cell is stretched, it will deform as shown in Fig. 3. The deformation of the cell can be achieved by three stages. In stage 1, we separate the cell into independent elements and tensile each element with a uniform stress, where the effect of the Poisson ratio of the materials is neglected. The elements with a lower elastic modulus (R_1) deform longer compared with the other elements (R_2). In stage 2, we connect the boundaries between two vertical elements and the interaction forces will compress the elements with a lower elastic modulus in the length direction, causing extension in the width direction as well. Then, in stage 3, interaction forces are applied on the connected boundaries between two horizontal

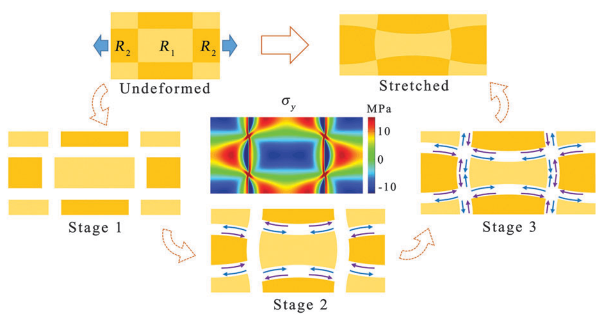

Fig. 3 Deforming process of a stretched periodic cell and the stress field σ_y (L_e/W_e = 2, E_1 = 1.44 GPa, E_2 = 2.88 GPa, ε = 10%).

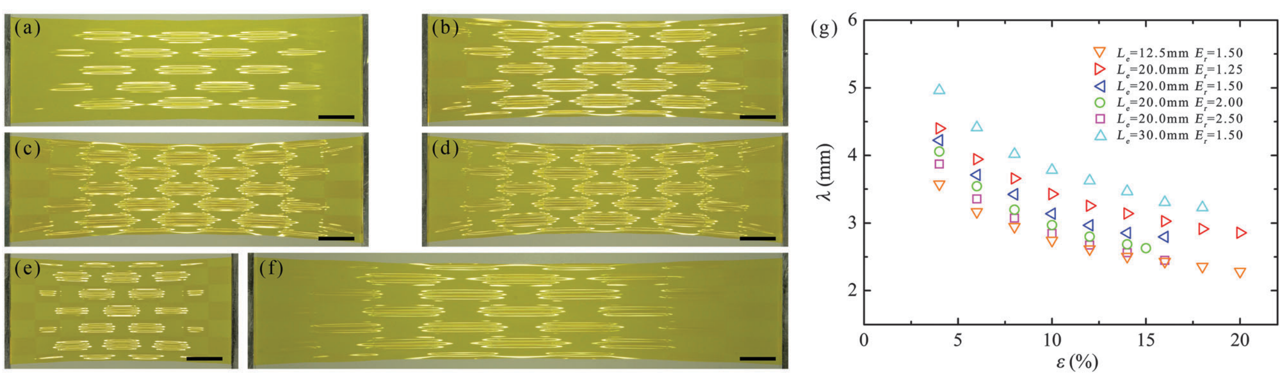

Fig. 2 Wrinkle patterns with different wavelengths for the structured films at 10% strain. The length of the element (L_e) is designed to be 20.0 mm with increasing ratios of elastic moduli of the two materials (E_r) (a) 1.25, (b) 1.50, (c) 2.00 and (d) 2.50, whose porosities in the structured element are 7.7%, 14.3%, 24.6% and 32.2%, respectively. L_e changes from (e) 12.5 mm to (f) 30.0 mm with a fixed E_r of 1.50. All scale bars are 20 mm. (g) Plot of wavelength λ against ε for the structured films above.

elements, leading to the compression in the width direction on the elements with lower elastic modulus. Thus, the element with lower elastic modulus (E_1) is under compression generated by the constraint from adjacent elements with contrasted elastic modulus, resulting in further wrinkling over a critical strain. On the other hand, tensile stress is generated in the element with high elastic modulus (E_2), preventing the formation of the wrinkles. The structured film under stretching finally displays periodic wrinkles with the same pattern as the elements.

Wrinkle characteristics

To characterize the wrinkles of the structured film, we propose a nonlinear mechanical model to describe the behavior of wrinkling. The periodic cell consisting of four elements ($2L_e \times 2W_e$, $L_e/W_e > 1$) is chosen, as shown in Fig. 1. The two types of elements in the cell, corresponding to the two regions R_1 and R_2, have different elastic moduli, E_1 and E_2 ($E_2 > E_1$), and the same Poisson ratio, $\nu = \nu_1 = \nu_2$, respectively. Now we consider the energy in the two regions. The total energy in region R_1 or R_2 consists of bending and stretching energies. It can be seen from Fig. 1b that most of the serious wrinkles are distributed in R_1, whereas they have been drastically weakened in R_2. The bending energy, which relates to the curvature in the width direction, is therefore much larger in R_1 than in R_2. Conversely, the stretching energy, which contributes to the gradient of out-of-plane displacement in the length direction, is larger in R_2 than in R_1. We have proved numerically that the bending energy of the film in R_1 and the stretching energy of the film in R_2 are dominant in the total energy when the value of L_e/W_e multiplied by E_r is less than or equal to 5. Thus, only the bending energy, U_1, in R_1 and the stretching energy, U_2, in R_2 are considered. According to previous studies,[12,23,34] the bending energy, U_1, in R_1 can be estimated by

$$U_1 \sim \frac{E_1 t^3}{(1-\nu^2)}\left(\frac{A}{\lambda^2}\right)^2 L_e W_e, \tag{1}$$

where λ and A are the wavelength and amplitude of the wrinkles, respectively, and t is the thickness of the film. The stretching energy, U_2, in R_2 can be estimated by

$$U_2 \sim T_2\left(\frac{A}{L_e}\right)^2 L_e W_e, \tag{2}$$

where T_2 is the tension in R_2. The strain in the two regions is assumed to be uniform and equal to the applied tensile strain, ε. Thus, T_2 in R_2 is expressed as $E_2\varepsilon t$. As wrinkles are triggered due to the in-plane mismatch of elastic modulus, it satisfies the condition of inextensibility in the width direction as (see ESI†)

$$\left(\frac{A}{\lambda}\right)^2 \sim \frac{E_r(E_r-1)}{(E_r+1)^2}\left(\frac{L_e}{W_e}\right)\varepsilon. \tag{3}$$

As a consequence, the bending energy in R_1 ($U_1 \propto \lambda^{-2}$) tends to favor a large wavelength, whereas the stretching energy in R_2 ($U_2 \propto \lambda^2$) is minimized when the wavelength vanishes. The competition between the two energies will result in wrinkling. The optimal wavelength is determined by the minimization of the total energy of the periodic cell, $\partial(U_1 + U_2)/\partial\lambda = 0$, which gives

$$\lambda \sim (1-\nu^2)^{-\frac{1}{4}} E_r^{-\frac{1}{4}} L_e^{\frac{1}{2}} t^{\frac{1}{2}} \varepsilon^{-\frac{1}{4}}. \tag{4}$$

From the scaling law, the wavelength of wrinkles on the structured film depends not only on the dimensions of the elements and the stretching strain but also on the material properties, especially the ratio of the elastic moduli of the two materials. The interaction between the materials with a contrasted in-plane elastic modulus determines the wrinkle pattern and location. A larger ratio of E_r will lead to a smaller wavelength of the wrinkles. Periodic wrinkles can be distributed in the local regions of a film whose wavelength is much smaller than the size of the whole film. Thus, wrinkles with a small wavelength can be achieved in desired local regions by designing the elastic moduli of materials in a controllable way. Substituting the expression of λ into eqn (3), the amplitude of wrinkles is obtained (see ESI†), but the accuracy of the scaling law for the amplitude of wrinkles is limited. Our scaling law is also suitable for the wrinkled films with compliant boundaries. Previous reports by Cerda *et al.*[12,23] showed that the wrinkle wavelength and amplitude of the clamped uniform film, distributed across the whole uniform film, have no relation to the elastic modulus of the material. When the two materials of the film have the same mechanical properties, periodic wrinkles in the local regions disappear since the amplitude equals zero (see ESI†), and the wrinkles across the whole film arise, whose wrinkle pattern is governed by the scaling law for uniform films.[12,23]

To verify the scaling law we proposed, we measure the wavelengths of wrinkles at different strains experimentally (Fig. 2g) and plot the dimensionless wavelength $\lambda_0 = \lambda(1-\nu^2)^{\frac{1}{4}}E_r^{\frac{1}{4}}L_e^{-\frac{1}{2}}t^{-\frac{1}{2}}$ as a function of $\varepsilon^{-\frac{1}{4}}$. As shown in Fig. 4, the data show a linear relationship with $\varepsilon^{-\frac{1}{4}}$, proving the accuracy of our theoretical scaling law for wavelength. We fit the data by linear function and obtain a constant 2.82 as the prefactor.

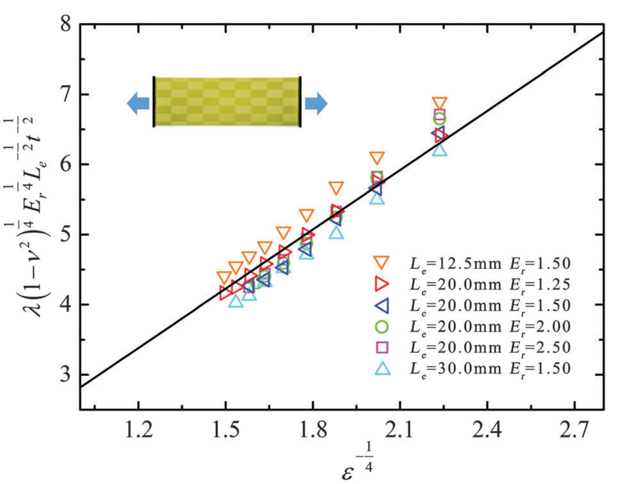

Fig. 4 Plot of the dimensionless wavelength $\lambda_0 = \lambda(1-\nu^2)^{\frac{1}{4}}E_r^{\frac{1}{4}}L_e^{-\frac{1}{2}}t^{-\frac{1}{2}}$ against $\varepsilon^{-\frac{1}{4}}$ for the structured films in experiment (Fig. 2). The applied tensile strain is up to 20%. Full line: scaling law $\lambda_0 = 2.82\varepsilon^{-\frac{1}{4}}$.

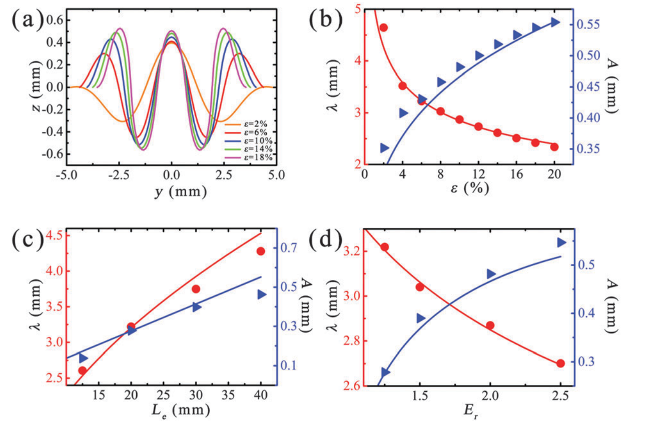

Fig. 5 (a) Cross profiles along the vertical central line of the wrinkled element at different strain levels (L_e = 20.0 mm, E_r = 2.00). Variations of wavelength and amplitude with increasing (b) strain ε (L_e = 20.0 mm, E_r = 2.00), (c) element length L_e (E_r = 1.25, ε = 10%) and (d) ratio of elastic moduli E_r (L_e = 20.0 mm, ε = 10%). W_e = 10.0 mm, t = 0.025 mm. The data are calculated by FEM based on a periodic cell and the lines are predicted by the theoretical scaling laws. The constant prefactors for the wavelength and amplitude are 2.63 and 2.04, respectively.

The wrinkling of a structured film under stretching is also modeled by using commercial FEM software ABAQUS (see ESI†). The numerical results by FEM postbuckling analysis agree well with the experimental results and verify that the scaling law for the structured film can be used to describe the characteristics of wrinkles in the experiment. As strain increases, a decreasing wavelength and increasing amplitude of the wrinkles are seen from the cross profiles of the wrinkled element (Fig. 5a), indicating the scaling relationships of $\lambda \sim \varepsilon^{-\frac{1}{4}}$ and $A \sim \varepsilon^{\frac{1}{4}}$ (Fig. 5b). By varying the length of element L_e keeping other parameters fixed, the wavelength and amplitude are increased with increasing L_e with the scaling relationships of $\lambda \sim L_e^{\frac{1}{2}}$ and $A \sim L_e$, respectively, as shown in Fig. 5c. According to the wrinkling physics of the interaction of contrasted materials, the wavelength and amplitude of wrinkles on the structured film can be tailored by designing different elastic moduli of materials (Fig. 5d).

When L_e/W_e or E_r becomes too large, *i.e.*, the element becomes too slender or the two materials become strongly mismatched, the bending and stretching energies in R_1 or R_2 have nearly the same magnitude, indicating that no energy can be neglected. The effect of L_e/W_e and E_r on the accuracy of our scaling law is therefore discussed. Our numerical results indicate that E_r should be always less than or equal to 5 in order to generate regular sine-shape wrinkles, and a larger E_r makes the wrinkles deform seriously and deviate the sine-shape morphology. We introduce a term, $E_r^{-\alpha}(\gamma\varepsilon)^{-\alpha\beta}$, into the scaling law in eqn (4) and give an improved scaling law to describe the wavelength of the wrinkles for the cases with large E_rL_e/W_e as

$$\lambda \sim [(1-\nu^2)E_rL_e^{-2}t^{-2}\varepsilon]^{-\frac{1}{4}}E_r^{-\alpha}(\gamma\varepsilon)^{-\alpha\beta}. \tag{5}$$

The parameters $\alpha = a(L_e/W_e - 1)^b$, $\beta = a(E_r - 1)^b$. a, b and γ are constants. By changing L_e/W_e or E_r from 1.25 to 5.00, we calculate the wavelength of wrinkles under stretching by FEM based on a periodic cell as shown in Fig. 6a, and finally obtain the parameters to be a = 0.16, b = 1.15 and γ = 2.59 with a prefactor of 2.77 by fitting all the data shown in Fig. 6b. The improved scaling law can predict the wavelength of the structured film for the cases with large E_rL_e/W_e well. When L_e/W_e or E_r is small, α or β is approximate to zero, then the improved scaling law in eqn (5) will approach the simple scaling law in eqn (4).

The wrinkling of a uniform film *via* the Poisson effect can be analogous to the uniform film bonded on an effective substrate.[12] Here, we also apply the model of a film-substrate structure to describe the wrinkling of the structured film, and the wrinkle wavelength caused by the contrasted materials [eqn (4)] is rewritten as

$$\lambda \sim \left(\frac{B_f}{E_rK_e}\right)^{\frac{1}{4}}, \tag{6}$$

where $B_f \sim (1-\nu^2)^{-1}E_ft^3$ is the bending stiffness of a thin film which could be approximately assumed to be made up of any material. E_f and ν are the elastic modulus and Poisson ratio of the assumed film, respectively. $E_rK_e \sim E_rT/L_e^2 = E_rE_f\varepsilon t/L_e^2$ is the stiffness of the effective substrate where T is the tension

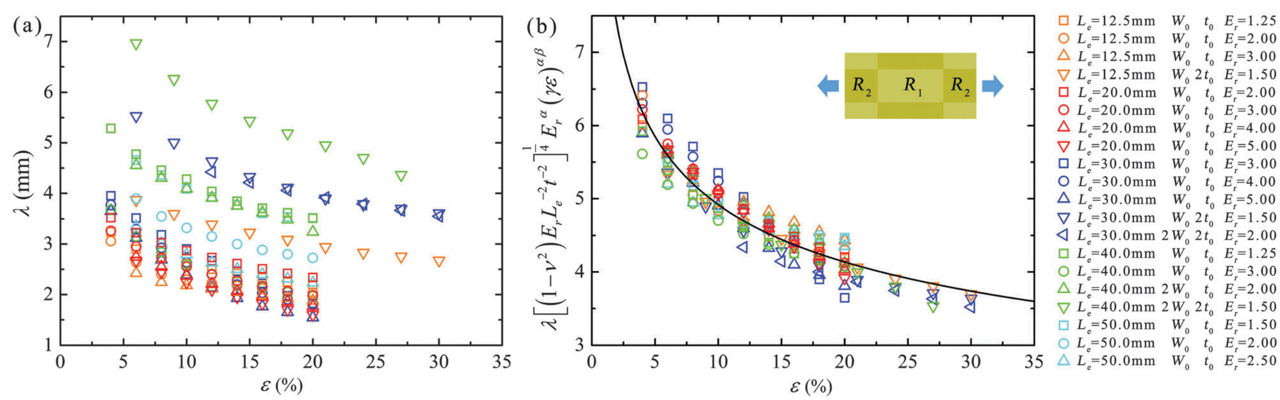

Fig. 6 Plots of (a) wavelength λ against ε and (b) dimensionless wavelength $\lambda_0 = \lambda[(1-\nu^2)E_rL_e^{-2}t^{-2}]^{\frac{1}{4}}E_r^{\alpha}(\gamma\varepsilon)^{\alpha\beta}$ against ε for various geometries and material properties. The data are calculated by FEM based on a periodic cell (full line: scaling law $\lambda_0 = 2.77\varepsilon^{-\frac{1}{4}}$). $\alpha = 0.16(L_e/W_e - 1)^{1.15}$, $\beta = 0.16(E_r - 1)^{1.15}$, γ = 2.59, W_0 = 10.0 mm and t_0 = 0.025 mm.

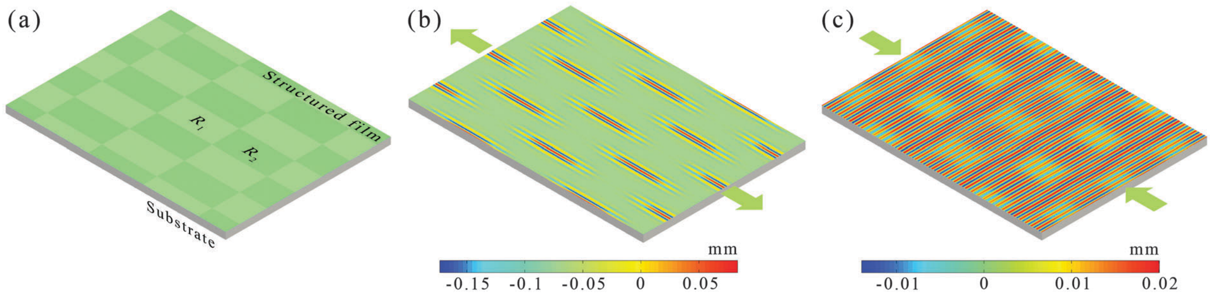

Fig. 7 (a) Structured thin film bonded on a compliant substrate. The surface of the heterogeneous film-substrate structure displays different periodic patterns at (b) tension strain 6% and (c) compressive strain −0.23%.

applied on the film. The stiffness of the effective substrate for clamped structured films is determined by both the heterogeneous materials (E_r) and size of the element in the structured film (L_e), whereas that for the clamped uniform films only depends on the length of the whole film, not on the elastic modulus of the uniform film.

Because the clamped ends of the whole structured film also provide a stiffness K_f by the Poisson effect of the whole film,[12] both the contrasted materials between the elements and the Poisson effect of the whole film are important factors to determine the effective elastic substrate in the film-substrate model. Wrinkling of the structured film is finally considered as the wrinkling of a uniform film on a composite substrate, which consists of a uniform substrate with stiffness K_f and periodic elements with stiffness E_rK_e superposed on the uniform substrate. Comparing the length of the whole film with that of the element, the films in Fig. 2 result in a large stiffness of the effective substrate K_f, which resists the deformation of the substrate, and the wrinkle pattern is therefore mainly triggered *via* the interaction of contrasted materials. When the elements in the film are small enough as compared to the length of the whole film that the effective substrate E_rK_e is large, the wrinkles *via* the Poisson effect are distributed with the same pattern as that of a uniform film, whereas the wrinkling *via* contrasted materials becomes very weak.

Heterogeneous film-substrate structure

We further find that the interaction between the in-plane mismatched materials is also indispensable to the wrinkling of the heterogeneous film-substrate structure, for example, a structured film bonded on a compliant substrate. As shown in Fig. 7a, a structured film, whose periodic element has the size of 20.0 × 10.0 × 0.025 mm (length × width × thickness), is bonded to a compliant substrate with a thickness of 2.5 mm. E_r is 2.00 and the compliant substrate has a low elastic modulus $E_s = 10^{-4}\ E_2$. Poisson ratios of the film and substrate are 0.31 and 0.45, respectively. The bottom surface of the substrate is constrained in the out-of-plane direction, and periodic conditions are applied on the four sides of the thin film and the substrate. We apply a displacement on the left and right sides to stretch or compress the whole film-substrate structure, setting other boundaries to be traction-free, and calculate the wrinkling by FEM postbuckling analysis. Different from no wrinkles on a uniform film-substrate structure under stretching, when this heterogeneous film-substrate structure is stretched uniaxially, wrinkles are formed on the surface of the film-substrate structure, parallel to the direction of tension, *via* the interaction of contrasted materials (Fig. 7b). The wrinkle pattern is similar to that of a free-standing structured film, as shown in Fig. 1b, but the wrinkle wavelength decreases at the same strain. Interestingly, when the external force turns to be compressive, another wrinkle pattern appears across the whole film-substrate structure (Fig. 7c). The wrinkle is perpendicular to the direction of compression, with a higher amplitude on the elements with high elastic modulus. Thus, applying a cyclic force on the heterogeneous film-substrate structure can trigger orthogonal wrinkles at different local regions of the structure. It is reported that two distinct regions of wrinkle morphology can be achieved on a unique surface by bonding the film on designed regions of the substrate.[18] This phenomenon can be considered as the wrinkling of the heterogeneous film-substrate structure, where the wrinkles in the unsupported region are triggered by the interaction of contrasted materials. Thus, new morphology of the wrinkle pattern on the film can be modified and controlled by taking advantage of the interaction of contrasted materials.

Conclusions

Structured films can be wrinkled in local regions of the film due to compressive stress *via* the interaction between materials with contrasted mechanical properties. A structured film can exhibit a periodic characteristic of wrinkles under stretching, and a set of scaling laws are able to characterize the wrinkle wavelength. The wrinkle wavelength and amplitude depend not only on the dimensions of elements and the stretching strain but also on the material properties, especially the ratio of the elastic moduli of the two materials. The interaction between the in-plane mismatched materials is also indispensable to the wrinkling of the film-substrate structure when the structured heterogeneous film is bonded on a compliant substrate. Various surface patterns of wrinkles can be generated by bonding a structured film on a substrate. Our work provides a potential method to generate controllable wrinkle patterns on heterogeneous films, which may have emerging applications in various disciplines.

Acknowledgements

Support from NSFC (Grant No. 11202025, 11290153 and 11472044) is acknowledged.

Notes and references

1 J. A. Rogers, T. Someya and Y. G. Huang, *Science*, 2010, **327**, 1603–1607.
2 D. H. Kim and J. A. Rogers, *Adv. Mater.*, 2008, **20**, 4887–4892.
3 A. B. Croll and A. J. Crosby, *Macromolecules*, 2012, **45**, 4001–4006.
4 J. M. Harris, J. Y. Huh, M. R. Semler, T. Ihle, C. M. Stafford, S. D. Hudson, J. A. Fagan and E. K. Hobbie, *Soft Matter*, 2013, **9**, 11568–11575.
5 M. R. Semler, J. M. Harris, A. B. Croll and E. K. Hobbie, *Phys. Rev. E: Stat., Nonlinear, Soft Matter Phys.*, 2013, **88**, 032409.
6 E. K. Hobbie, D. O. Simien, J. A. Fagan, J. Y. Huh, J. Y. Chung, S. D. Hudson, J. Obrzut, J. F. Douglas and C. M. Stafford, *Phys. Rev. Lett.*, 2010, **104**, 125505.
7 C. M. Stafford, C. Harrison, K. L. Beers, A. Karim, E. J. Amis, M. R. Vanlandingham, H. C. Kim, W. Volksen, R. D. Miller and E. E. Simonyi, *Nat. Mater.*, 2004, **3**, 545–550.
8 J. Huang, M. Juszkiewicz, W. H. de Jeu, E. Cerda, T. Emrick, N. Menon and T. P. Russell, *Science*, 2007, **317**, 650–653.
9 B. Li, Y. P. Cao, X. Q. Feng and H. Gao, *Soft Matter*, 2012, **8**, 5728–5745.
10 J. Dervaux, Y. Couder, M. A. Guedeau-Boudeville and M. Ben Amar, *Phys. Rev. Lett.*, 2011, **107**, 018103.
11 W. T. S. Huck, *Nat. Mater.*, 2005, **4**, 271–272.
12 E. Cerda and L. Mahadevan, *Phys. Rev. Lett.*, 2003, **90**, 074302.
13 E. Cerda, *J. Biomech.*, 2005, **38**, 1598–1603.
14 J. R. Blandino, J. D. Johnston and U. K. Dharamsi, *J. Spacecr. Rockets*, 2002, **39**, 717–724.
15 Y. W. Wong and S. Pellegrino, *J. Mech. Mater. Struct.*, 2006, **1**, 3–25.
16 D. Yan, K. Zhang, F. Peng and G. Hu, *Appl. Phys. Lett.*, 2014, **105**, 071905.
17 C. F. Guo, V. Nayyar, Z. Zhang, Y. Chen, J. Miao and R. Huang, and Q. Liu, *Adv. Mater.*, 2012, **24**, 3010–3014.
18 Y. Ebata and A. J. Crosby, *Soft Matter*, 2014, **10**, 1963–1968.
19 Y. Ebata, A. B. Croll and A. J. Crosby, *Soft Matter*, 2012, **8**, 9086–9091.
20 B. Li, F. Jia, Y. P. Cao, X. Q. Feng and H. Gao, *Phys. Rev. Lett.*, 2011, **106**, 234301.
21 P. Muller and J. Kierfeld, *Phys. Rev. Lett.*, 2014, **112**, 094303.
22 J. Hure, B. Roman and J. Bico, *Phys. Rev. Lett.*, 2012, **109**, 054302.
23 E. Cerda, K. Ravi-Chandar and L. Mahadevan, *Nature*, 2002, **419**, 579–580.
24 Z. Y. Huang, W. Hong and Z. Suo, *J. Mech. Phys. Solids*, 2005, **53**, 2101–2118.
25 V. Nayyar, K. Ravi-Chandar and R. Huang, *Int. J. Solids Struct.*, 2014, **51**, 1847–1858.
26 S. Cai, D. Breid, A. J. Crosby, Z. Suo and J. W. Hutchinson, *J. Mech. Phys. Solids*, 2011, **59**, 1094–1114.
27 K. Zhang, H. Duan, B. L. Karihaloo and J. Wang, *Proc. Natl. Acad. Sci. U. S. A.*, 2010, **107**, 9502–9506.
28 Y. Su, B. Ji, K. C. Hwang and Y. Huang, *J. Mech. Phys. Solids*, 2012, **60**, 1771–1790.
29 R. Blossey, *Nat. Mater.*, 2003, **2**, 301–306.
30 H. Liang and L. Mahadevan, *Proc. Natl. Acad. Sci. U. S. A.*, 2009, **106**, 22049–22054.
31 J. H. Lee, H. W. Ro, R. Huang, P. Lemaillet, T. A. Germer, C. L. Soles and C. M. Stafford, *Nano Lett.*, 2012, **12**, 5995–5999.
32 W. T. S. Huck, N. Bowden, P. Onck, T. Pardoen, J. W. Hutchinson and G. M. Whitesides, *Langmuir*, 2000, **16**, 3497–3501.
33 N. Bowden, S. Brittain, A. G. Evans, J. W. Hutchinson and G. M. Whitesides, *Nature*, 1998, **393**, 146–149.
34 A. Takei, F. Brau, B. Roman and J. Bico, *Europhys. Lett.*, 2011, **96**, 64001.